Eikonal calculations for high-energy electron-nucleus scattering

J. Diarmuid Murphy
*Department of Physics, Catholic University of America, Washington, D.C. 20064**

H. Überall
*Department of Physics, Catholic University of America, Washington, D.C. 20064**
and Naval Research Laboratory, Washington, D.C. 20375

(Received 25 June 1974)

The complete electron-nucleus cross section, containing both longitudinal and transverse interactions, has been obtained for elastic as well as inelastic scattering using the eikonal wave functions of Yennie *et al.* This approach is based on the distorted-wave Born approximation, and retains only the leading term in an asymptotic expansion (in inverse powers of momentum transfer times nuclear radius) of the eikonal integrals. The method should be valid at electron energies above 2–300 MeV, and should constitute an improvement over the phase-shift method when the latter becomes inaccurate above 4–500 MeV. A simple collective nuclear model for magnetic transitions is also given, which contains the rotational collective flow of nuclear charge.

[NUCLEAR REACTIONS Electron scattering ^{27}Al, ^{51}V, ^{115}In, ^{208}Pb, ^{209}Bi calculated elastic, inelastic magnetic form factors using eikonal method.]

I. INTRODUCTION

Electron-nucleus scattering experiments have provided much useful information concerning nuclear structure.[1]

The electron-nucleus interaction is well understood. The electromagnetic field of the incident electron interacts with the charge and current of the target nucleus. This interaction is weak and is given by quantum electrodynamics.

At large momentum transfer the contributions from the higher-order nuclear charge and current multipoles can be enhanced. Also at large scattering angles the contribution from the transverse multipoles can be increased relative to that from the charge multipoles.[2–7]

Elastic magnetic electron scattering has proven useful for studying the nuclear ground-state current and magnetization distributions. Measurements of the magnetic multipole form factors of ^{27}Al, ^{51}V, and ^{209}Bi, and corresponding calculations have shown that scattering from very high magnetic moments may prominently contribute and even predominate over Coulomb scattering at scattering angles much less than 180°.[3,5,7]

For an accurate analysis of such data, the plane-wave Born approximation (or PWBA), which assumes that both the initial and final electrons are plane waves, is inadequate even for a nucleus as light as ^{27}Al.[8]

In reality, the electron wave function is significantly distorted by the electromagnetic field of the nucleus. The purpose of this work is to compute the electron-nucleus scattering cross section with electron wave functions that take this "Coulomb distortion" effect into account.

We will consider only a one-photon exchange process, i.e., treat the nuclear transition to lowest order in $Z\alpha$. However, the incident and outgoing electron waves will be treated as distorted plane waves. This approach is known as first-order distorted-wave Born approximation (or DWBA).[1]

Most approaches to the problem of Coulomb distortion can be classified as either partial-wave analyses or WKB methods. The latter apply only in the high-energy regime, where $k_1 R \gg 1$ (k_1 is the incident electron momentum, R is the electromagnetic nuclear radius).

In the phase-shift analysis of either elastic or inelastic scattering from an extended nucleus, the radial electron wave functions are found by numerically integrating a pair of coupled differential equations representing the Dirac equation for an electron in a centrally symmetric static potential. A potential resulting only from the monopole part of the nuclear ground-state charge density is chosen, since higher multipole potentials will couple the partial waves and result in a very large system of coupled differential equations. This restriction favors a choice of target nuclei near closed shells.

When high incident electron energies are considered ($E_1 > 300$ MeV), many partial waves (more than 30) will contribute. The resulting numerical calculations are quite lengthy. Due to sensitive cancellation effects in the partial-wave series they must be performed very accurately. These and other difficulties have been discussed by Drech-

sel.[9] In more recent work by Gargaro and Onley,[10,11] Glossmann and Toepffer,[12] Heisenberg and Sick,[13] and Wright and Prewitt,[7] improved methods for computing the integrals of the radial wave functions have been worked out.

As an alternative to the method of partial waves, which should replace the latter at high energies, several methods closely related to the classical eikonal method of geometrical optics[14] have been developed. It was reasoned that in the high-energy (or short-wavelength) limit, where quantities such as the potential energy, the modulus of the wave function, and the local wave number are slowly varying over one wavelength, the electron can be approximated by a plane wave of modified amplitude and phase.

The three main approaches are due to (1) Schiff,[15] Saxon,[16,17] and Tiemann[18]; (2) Glauber[19] and Baker[20]; and (3) Yennie, Boos, and Ravenhall.[21]

Yennie *et al.* devised an eikonal approximation for computing accurate electron wave functions in the vicinity of the nucleus, and applied it to a computation of Coulomb scattering cross sections. This method is equally applicable to elastic or inelastic processes. It has been specialized for the case of nuclear charge densities which are either Fermi or can be expressed as a series of derivatives of the Fermi density.[22-26]

In the present work, we have applied this high-energy approximation to the complete electron-nucleus interaction (including the transverse interaction) for the usual one-photon exchange process.

In order to check on the accuracy of our approach, we use two recent computer codes that have been developed for carrying out partial-wave analyses of electron-nucleus scattering: (1) HEINEL, which computes the inelastic electric (without spin-flip) scattering cross section[13]; and (2) MAGEL, which computes the elastic magnetic scattering cross section.[6,7]

The eikonal scattering cross sections which we will derive are found to have a region of validity which is a function of the incident electron energy E_1, scattering angle θ, and the multipolarity of the nuclear moment (ground state or transition) of interest.

In general θ must be large enough so that $qR \gg 1$ (q being the momentum transfer), i.e., $\theta > 1/k_1R$. This means that if electrons of energy $E_1 \geq 200$ MeV are scattered off medium and heavy nuclei, we must have $\theta \gtrsim 30°$. Below such a critical angle (which increases with multipolarity), the eikonal cross sections are found to deteriorate abruptly. The latter were obtained following a sequence of asymptotic expansions in inverse powers of qR. The Coulomb (C), transverse electric (TE), and transverse magnetic (TM) scattering amplitudes are found as single integrals over the nuclear radial coordinate.

The exact limits of validity for the eikonal approach cannot be cleanly stated. The PWBA cross section, calculated[1] with a modified q, can often be used as a check in the region of diffraction maxima. However, the accuracy of the eikonal method does increase with increasing energy, while the opposite holds for phase-shift analysis.

II. EIKONAL WAVE FUNCTIONS

The eikonal approximation is motivated by some general features of electron-nucleus scattering at high incident electron energies, as follows:

(1) The part of the differential scattering cross section useful for investigating nuclear structure occurs at large scattering angles, many times the classical scattering angle. This large-angle scattering comes from a high momentum-transfer collision which happens in the vicinity of the nucleus.

(2) The incident electron suffers many small collisions as it encounters the smooth long-range tail of the Coulomb potential due to an extended nucleus. The electron's initial and final wave functions are gradually distorted as it approaches the target. Near the nucleus the Coulomb potential is still smooth and the potential energy is small compared to the electron's total energy, so that the electron's wave function may be represented as a plane wave of modified amplitude and wave number.

It is assumed that the change in local wave number is small over one wavelength; if k_1 is the incident electron's momentum, and $V(r)$ the spherically symmetrical Coulomb potential it traverses, then $\partial V/\partial r \ll k_1^2$. For a nucleus of charge Z and radial extension of order R, this implies $\gamma/(k_1R)^2 \ll 1$, where $\gamma = Ze^2$.

After solving the Dirac equation for an electron in a spherically symmetric external electrostatic potential, the lowest-order eikonal electron wave function is obtained as follows[21]:

$$\Psi^{(+)}_{R,L}(\vec{k}_1) = u^{(+)}_{R,L}(\vec{k}_1) e^{iS^{(+)}(\vec{k}_1)} \tag{1}$$

with

$$u^{(+)}_{R,L}(\vec{k}_1) = (k'/k)\{[1 + a(\vec{k}_1' \cdot \vec{r})^2 - a(\vec{k}_1' \times \vec{r})^2 + 3b(\vec{k}_1' \cdot \vec{r}) - 10c(\vec{k}_1' \cdot \vec{r})(\vec{k}_1' \times \vec{r})^2] \mp (\vec{\sigma} \cdot \vec{r})[\tfrac{1}{2}ak'(\vec{k}_1' \cdot \vec{r}) + bk' - 2ck'(\vec{k}_1' \times \vec{r})^2]\} v_{R,L}(\hat{k}_1) \tag{2}$$

and

$$S^{(+)}(\vec{k}_1) = S(0) + \vec{k}_1' \cdot \vec{r} - \tfrac{1}{6}a\vec{k}_1' \cdot \vec{r}[3k'^2r^2 - 2(\vec{k}_1' \cdot \vec{r})^2] - b(\vec{r} \times \vec{k}_1')^2 + c(\vec{r} \times \vec{k}_1')^4 . \quad (3)$$

The superscript (+) denotes an incident plane wave plus outgoing spherical wave; subscripts R or L refer to right-handed or left-handed electrons. Furthermore,

$$v_R = \begin{pmatrix} \cos\tfrac{1}{2}\theta \\ \sin\tfrac{1}{2}\theta e^{i\phi} \end{pmatrix}, \quad v_L = \begin{pmatrix} -\sin\tfrac{1}{2}\theta e^{i\phi} \\ \cos\tfrac{1}{2}\theta \end{pmatrix},$$

where (θ, ϕ) denote the direction of the electron momentum $\vec{k}_1$ and

$$\vec{k}' = \vec{k}[1 - V(0)/E_1] ,$$

$$V(r) = -4\pi\gamma\left[r^{-1}\int_0^r r'^2\rho(r')dr' + \int_r^\infty r'\rho(r')dr'\right],$$

with $\rho(r)$ the nuclear charge density.

The parameter a is defined by the assumption that near the origin (center of the nucleus),

$$V(r) = V(0) + \tfrac{1}{2}ak'^3r^2 + \cdots .$$

Further,

$$b = (\pi\gamma/k'^2)\int_0^\infty \rho(r)dr$$

and

$$c = -(\pi\gamma/8k'^4)\int_0^\infty r^{-1}(\partial\rho/\partial r)dr .$$

Another type of scattering wave function with superscript (−) also arises, containing incident spherical plus outgoing plane wave. By reversing the sign of S, the plus-type solutions are converted to the minus type with final momentum the negative of $\vec{k}_1$.

To obtain the minus-type scattering wave function from the plus type in Eq. (1) we must change the signs of b and c since $\psi^{(-)}_{\vec{k},\vec{\sigma}} = \psi^{(+)}_{-\vec{k},-\vec{\sigma}}$.

III. ELECTRON-NUCLEUS SCATTERING CROSS SECTIONS

We now wish to compute the electron-nucleus scattering cross section with one-photon exchange, using distorted electron wave functions. Our discussion will be general enough to hold for both elastic and inelastic scattering of arbitrary multipole order. Nuclear recoil will be neglected.

We further assume that the ground-state charge density is spherically symmetric (as done in the preceding section) and that the excited state charge density is not significantly different from that of the ground state. This latter assumption allows us to use initial and final electron wave functions $\psi^{(+)}_{\vec{k}1}$, $\psi^{(-)}_{\vec{k}2}$ containing the same set of distortion parameters k', a, b, and c.

For the derivation of the electron-nucleus interaction matrix element one can rigorously start from quantum field theory as done by Reynolds.[27] It is equivalent to start from a classical retarded electron-nucleus interaction as has been explicitly shown.[27,28] We will take the latter approach.

The complete electron-nucleus interaction is determined by three quantities which describe the electromagnetic properties of the nucleus: (1) the nuclear charge density $e\rho(r)$ normalized according to $\int\rho(\vec{r})d\vec{r} = Z$; (2) the nuclear (convection) current density $e\vec{J}_c(\vec{r})$; and (3) the nuclear (spin) magnetization density $e\vec{\mu}_s(\vec{r})$. The latter two may be combined into a total current, $\vec{J}(\vec{r}) = \vec{J}_c(\vec{r}) + \vec{\nabla} \times \vec{\mu}_s(\vec{r})$.

The process of an electron passing through the nuclear electromagnetic field can then be described by an interaction Hamiltonian density function $H_I = H_C + H_T$ where the longitudinal (or Coulomb) part is

$$H_C = e\int\rho(\vec{r})\Phi(\vec{r})d^3r$$

and the transverse part is

$$H_T = -e\int[\vec{J}_c(\vec{r}) \cdot \vec{A}(\vec{r}) + \vec{\mu}_s(\vec{r}) \cdot \vec{\nabla} \times \vec{A}(\vec{r})]d^3r .$$

Here $(\vec{A}, i\Phi)$ represents the classical electromagnetic field due to the electron. Passing to the quantum-mechanical limit we can expand the nuclear charge and current operators in spherical multipoles:

$$\rho^{\text{op}}(\vec{r}) = \sum_{lm}\tilde{\rho}_{lm}(r)Y^*_{lm}(\hat{r})$$

and

$$\vec{J}^{\text{op}}(\vec{r}) = \sum_{ll'm}\tilde{J}_{ll'm}(r)\vec{Y}^m_{ll'}{}^*(\hat{r}) .$$

The one-photon-exchange electron-nucleus scattering amplitude is now given by[1]

$$\langle J_fM_f|H_I^{\text{op}}|J_iM_i\rangle = \frac{4\pi ie\omega}{\hat{J}_f}\sum_{LL'M}(J_iM_i, LM|J_fM_f)\int r^2dr\int d^3r'\phi_{L'}(r,r') \times[\delta_{LL'}\rho_L^{if}(r)\rho_e(\vec{r}')Y^*_{LM}(\hat{r}') - J^{if}_{LL'}(r)\vec{j}_e(\vec{r}') \cdot \vec{Y}^{M*}_{LL'}(\hat{r}')], \quad (4)$$

where J_iM_i (J_fM_f) are the initial (final) nuclear spins, with $\phi_{L'}(r,r')=j_{L'}(\omega r_<)h_L^{(1)}(\omega r_>)$, where $r_<=\min(r,r')$ etc. All of the nuclear dynamics are contained in the nuclear transition densities $\rho_L^{if}(r)$, $J_{LL'}^{if}(r)$, being the reduced matrix elements of $\tilde{\rho}_{LM}$ and $\tilde{J}_{LL'M}$, respectively.

The electron densities $\rho_e(\vec{r}')$ and $\vec{j}_e(\vec{r}')$ can be expressed in terms of plane waves (PWBA), phase-shifted plane waves (DWBA), or by some high-energy approximation—in our case the eikonal method.

We consider that the initial electron beam is unpolarized, and the polarization of the electron beam in its final state is undetected. It follows that

$$\frac{d\sigma}{d\Omega}=\frac{1}{2}\left(\frac{E_2}{2\pi}\right)^2\frac{1}{\hat{J}_i^2}\sum_{m_1m_2}\sum_{LM}\left|\sum_\tau H_{LM}^\tau\right|^2, \tag{5}$$

where $\langle J_fM_f|H_I^{\rm op}|J_iM_i\rangle=\sum_{\tau LM}(\hat{L}/\hat{J}_f)(J_iM_i,\,LM|J_fM_f)\times H_{LM}^\tau$, with $\tau=C$, TE, TM, E_2 being the final electron energy, and $\hat{J}_i=(2J_i+1)^{1/2}$, etc.

In the sum over τ, Coulomb (C) and transverse electric (TE) terms, for a given multipolarity L, will in general interfere unlike in a PWBA analysis. For nuclear states of well-defined parity, the electric and TM (transverse magnetic) terms, being of opposite parity, will not interfere.

We will now utilize the eikonal electron wave functions to obtain the Coulomb and transverse amplitudes. The scattering amplitude in Eq. (5) may be evaluated as follows: First, the integral over $\vec{r}'$ is performed. Next:

(1) Calling $\mu'=\cos\theta'$, $\int d\mu'$ is carried out by repeated use of integration by parts. An asymptotic series in inverse powers of $q'R$ $\{q'=q[1-V(0)/E]\}$ is thereby developed. Only the first term in this series is retained.

(2) $\int d\phi'$ is approximated analytically by neglecting small terms.

(3) $\int dr'$ is done similarly as was $\int d\mu'$. Successive use of integration by parts yields an asymptotic series in inverse powers of $(q'R)$ and only the first nonzero term is retained.

The remaining integral over the nuclear radial coordinate r is then evaluated on a digital computer. Since we desire to preserve some generality as far as the analytical forms of the nuclear charge and current densities are concerned, we do not adopt the contour integral techniques employed in Refs. 22–26. Our final expression for the Coulomb amplitude is

$$H_{LM}^C=4\pi^{3/2}e^2\delta_{M,0}\int_0^\infty r^2dr\rho_L^{if}(r)\times\sum_{\epsilon=\pm1}\epsilon\frac{F^C(r,\epsilon)G_L(r,\epsilon)}{[iq'C(r,\epsilon)]^2} \tag{6}$$

with

$$F^C(r,\epsilon)=(k'/k)^2\cos\tfrac{1}{2}\theta\, e^{i[q'r\epsilon+\Phi(r,\epsilon)]}\,\alpha(r,\epsilon),$$

appearing in Eq. (6) after integration over ϕ' and having been evaluated at $\mu'=\epsilon$, as is the following (using $\vec{K}'=\vec{k}_1'+\vec{k}_2'$):

$$\Phi(r,\epsilon)=2S(0)-\epsilon a[\tfrac{1}{2}q'k'^2-q'^3/12]r^3-\tfrac{1}{2}bK'^2r^2+\tfrac{1}{8}cK'^4r^4,$$

$$\alpha(r,\epsilon)=1+3\epsilon bq'r+a(q'^2-2k'^2)r^2-\tfrac{1}{4}\epsilon cq'K'^2r^3,$$

$$G_L(r,\epsilon)=\sum_{\nu=0}^{L}(-1)^\nu[iq'rE(r,\epsilon)]^{-\nu-1}\left[\frac{\partial^\nu P_L(\mu)}{\partial\mu^\nu}\right]_{\mu=\epsilon},$$

$$E(r,\epsilon)=1+B(r,\epsilon)+\tfrac{1}{2}R(r,\epsilon),$$

$$B(r,\epsilon)=-a(\tfrac{1}{2}k'^2-\tfrac{1}{4}q'^2)r^2+\epsilon bq'r-\tfrac{1}{2}\epsilon cq'K'^2r^3,$$

$$R(r,\epsilon)=-\tfrac{1}{2}aK'^2r^2-\epsilon bK'^2\frac{r}{q'}+\epsilon c(2k'^2-\tfrac{3}{2}q'^2)\frac{r^3}{q'},$$

and

$$C(r,\epsilon)=\epsilon-a\epsilon r^2(\tfrac{3}{2}k'^2-\tfrac{1}{4}q'^2)-\frac{brK'^2}{q'}+\frac{\frac{1}{2}cr^3K'^4}{q'}.$$

The transverse electric and magnetic amplitudes are given as

$$(H_{LM}^{\rm TE})_{RR}=-(2\pi)^{3/2}\frac{e^2}{\hat{L}}\left(\frac{k'}{k}\right)^2\delta_{M,\pm1}\times\sum_{L'=L\pm1}\int_0^\infty r^2drJ_{LL'}^{if}(r)\sum_{\epsilon=\pm1}\epsilon[iq'C(r,\epsilon)]^{-2}e^{i[q'r\epsilon+\Phi(r,\epsilon)]}(1+M\sin\tfrac{1}{2}\theta)$$
$$\times\Big[-M\hat{L}'X_{L'}(r,\epsilon)(L'0,11\,|\,L1)+\frac{2}{\hat{L}'}\Big(Z_{L'+1}(r,\epsilon)\{(L'+1)(L'0,11\,|\,L1)+[\tfrac{1}{2}L'(L'+1)]^{1/2}(L'1,10\,|\,L1)\}$$
$$+Z_{L'-1}(r,\epsilon)\{L'(L'0,11\,|\,L1)-[\tfrac{1}{2}L'(L'+1)]^{1/2}(L'1,10\,|\,L1)\}\Big)\Big] \tag{7}$$

and

$$(H_{LM}^{\rm TM})_{RR}=(2\pi)^{3/2}\frac{e^2}{\hat{L}}\left(\frac{k'}{k}\right)^2\delta_{M,\pm1}\int_0^\infty r^2drJ_{LL}^{if}(r)\sum_{\epsilon=\pm1}\epsilon[iq'C(r,\epsilon)]^{-2}e^{i[q'r\epsilon+\Phi(r,\epsilon)]}(1+M\sin\tfrac{1}{2}\theta)$$
$$\times\Big\{2^{-1/2}M\hat{L}X_L(r,\epsilon)-\frac{2^{1/2}}{\hat{L}}[LZ_{L+1}(r,\epsilon)+(L+1)Z_{L-1}(r,\epsilon)]\Big\} \tag{8}$$

for the case of right-handed (subscript R) electrons remaining right handed, e.g., with

$$X_{L'}(r,\epsilon)=\alpha(r,\epsilon)G_{L'}(r,\epsilon),$$
$$Z_{L'}(r,\epsilon)=rN(r,\epsilon)G_{L'}(r,\epsilon),$$
$$N(r,\epsilon)=\tfrac{1}{2}a\epsilon k'^2 r\sin\tfrac{1}{2}\theta+bk'-2ck'^3r^2\cos^2\tfrac{1}{2}\theta.$$

It is found that in our high-energy limit, electron spin-flip does not occur, as a consequence of the high-energy representation used, in which the only Dirac matrices (1 and $\vec{\alpha}$) occuring in the interaction, Eq. (4), are both diagonal. From this fact, and from symmetry considerations, one has

$$\begin{aligned}(H^{\mathrm{TE}}_{L,\pm1})_{RR}&=-(H^{\mathrm{TE}}_{L,\mp1})_{LL},\\ (H^{\mathrm{TM}}_{L,\pm1})_{RR}&=(H^{\mathrm{TM}}_{L,\mp1})_{LL}.\end{aligned}\tag{9}$$

These symmetries enable us to now write the electric and magnetic differential scattering cross sections corresponding to the Lth multipole order as

$$\left(\frac{d\sigma}{d\Omega}\right)^E_L=\frac{1}{2\hat{J}_i^{\,2}}\left(\frac{E_2}{2\pi}\right)^2\left[2\left|(H^{\mathrm{C}}_{L,0})_{RR}\right|^2+2\left|(H^{\mathrm{TE}}_{L,1})_{RR}\right|^2+2\left|(H^{\mathrm{TE}}_{L,-1})_{RR}\right|^2\right]\tag{10}$$

and

$$\left(\frac{d\sigma}{d\Omega}\right)^M_L=\frac{1}{2\hat{J}_i^{\,2}}\left(\frac{E_2}{2\pi}\right)^2\left[2\left|(H^{\mathrm{TM}}_{L,1})_{RR}\right|^2+2\left|(H^{\mathrm{TM}}_{L,-1})_{RR}\right|^2\right].\tag{11}$$

To explicitly evaluate the cross sections, two further steps are necessary. First, we must utilize models for the nuclear charge and current densities $\rho^{if}_L(r)$, $J^{if}_{L,L\pm1}(r)$, and $J^{if}_{L,L}(r)$. Secondly, a stable numerical algorithm is needed which will accurately integrate the oscillating functions found in the scattering amplitudes.

IV. NUCLEAR MODELS

Magnetic scattering at high values of q, as we will discuss in the next section, can be used to probe the spatial distribution of the magnetic moments, and in particular the effects of adding neutrons in the outermost shells where presumably magnetic effects predominantly originate.

Of considerable interest for decoupling the effect of Coulomb distortion is the ratio

$$f_c(q,E)=\frac{(d\sigma/d\Omega)^{\mathrm{DWBA}}}{(d\sigma/d\Omega)^{\mathrm{PWBA}}}.\tag{12}$$

In transverse scattering at high values of the momentum transfer, the orbital and spin currents contribute to the cross section in *a priori* unknown amounts and a model-independent evaluation of the correction factor $f_c(q,E)$ is difficult to obtain.[9] Thus for the incident electron energies and scattering angles of interest in this work ($E_1>200$ MeV, $\theta>30^\circ$), experiments should be compared directly with nuclear model calculations where distorted electron waves are used.

Of most interest to us are medium and heavy nuclei where Coulomb distortion effects play a large role. Due to the energy resolution limits of existing linear electron accelerators, the energy levels that have been most extensively studied in electron scattering are well-separated single-particle levels in light nuclei, and collective levels in medium to heavy nuclei.

We will apply (1) the single-particle shell model[29] to elastic magnetic scattering, and (2) a generalization of the Tassie[30] collective/phenomenological model to transverse inelastic scattering. In the first case we will be treating nuclei with closed shells plus or minus one valence particle, and in both cases nuclei with spherically symmetric ground-state charge densities.

In Eq. (4) it is convenient to define a spin current operator as

$$\vec{\mathrm{J}}^{\mathrm{op}}_s(\vec{\mathrm{r}})=\vec{\nabla}\times\vec{\mu}^{\mathrm{op}}_s(\vec{\mathrm{r}})\tag{13}$$

with

$$\vec{\mathrm{J}}^{\mathrm{op}}(\vec{\mathrm{r}})=\vec{\mathrm{J}}^{\mathrm{op}}_c(\vec{\mathrm{r}})+\vec{\mathrm{J}}^{\mathrm{op}}_s(\vec{\mathrm{r}}),\tag{14}$$

and to express the moments of $\vec{\mathrm{J}}^{\mathrm{op}}_s(\vec{\mathrm{r}})$ in terms of the moments of $\vec{\mu}^{\mathrm{op}}_s(\vec{\mathrm{r}})$ which in turn can be calculated from some physical model:

$$J^{if}_{sL,L+1}(r)=-i\frac{L^{1/2}}{\hat{L}}\left(\frac{d}{dr}-\frac{L}{r}\right)\mu^{if}_{sL,L}(r),\tag{15}$$

$$J^{if}_{sL,L}(r)=-i\left[\frac{L^{1/2}}{\hat{L}}\left(\frac{d}{dr}+\frac{L+2}{r}\right)\mu^{if}_{sL,L+1}(r)+\frac{(L+1)^{1/2}}{\hat{L}}\left(\frac{d}{dr}-\frac{L-1}{r}\right)\mu^{if}_{sL,L-1}(r)\right],\tag{16}$$

and

$$J^{if}_{sL,L-1}(r)=-i\frac{(L+1)^{1/2}}{\hat{L}}\left(\frac{d}{dr}+\frac{L+1}{r}\right)\mu^{if}_{sL,L}(r).\tag{17}$$

For the single-particle shell model, in calculating the nuclear matrix elements of $\vec{\mathrm{J}}^{\mathrm{op}}_c(r)$ and $\vec{\mathrm{J}}^{\mathrm{op}}_s(r)$ for nuclei with closed shells plus or minus one particle, we need only compute the single-odd-particle matrix elements. The outcome is that for oscilla-

tor shells with $n=1$:

$$J_{sL,L}(r)=\frac{-i}{rb^2}R_{1l}{}^2(r)\left[\frac{\mu}{4m}\left(\frac{6}{\pi}\right)^{1/2}(-1)^l\hat{l}^2\hat{j}^2\right]$$
$$\times\left\{L^{1/2}[b^2(2l+L+2)-2r^2](2L+3)\begin{Bmatrix} l & l & L+1\\ \frac{1}{2} & \frac{1}{2} & 1\\ j & j & L\end{Bmatrix}\begin{pmatrix} l & L+1 & l\\ 0 & 0 & 0\end{pmatrix}\right.$$
$$\left.+(L+1)^{1/2}[b^2(2l-L+1)-2r^2](2L-1)\begin{Bmatrix} l & l & L-1\\ \frac{1}{2} & \frac{1}{2} & 1\\ j & j & L\end{Bmatrix}\begin{pmatrix} l & L-1 & l\\ 0 & 0 & 0\end{pmatrix}\right\} \tag{18}$$

with nucleon magnetic moment μ and mass m, and

$$J_{cL,L}(r)=\frac{-i}{rb^2}R_{1l}{}^2(r)(-1)^{l+j-1/2}(2\pi^{1/2}m)^{-1}\hat{j}^2\hat{L}^2\begin{Bmatrix} l & j & \frac{1}{2}\\ j & l & L\end{Bmatrix}$$
$$\times\left\{(l+1)(-r^2)\begin{Bmatrix} L & 1 & L\\ l & l & l+1\end{Bmatrix}\frac{\begin{pmatrix} l & L & l+1\\ 0 & 0 & 0\end{pmatrix}}{\begin{pmatrix} l+1 & 1 & l\\ 0 & 0 & 0\end{pmatrix}}+l[(2l+1)b^2-r^2]\begin{Bmatrix} L & 1 & L\\ l & l & l-1\end{Bmatrix}\frac{\begin{pmatrix} l & L & l-1\\ 0 & 0 & 0\end{pmatrix}}{\begin{pmatrix} l-1 & 1 & l\\ 0 & 0 & 0\end{pmatrix}}\right\}, \tag{19}$$

b being the oscillator parameter, and R_{nl} the radial wave function.

Inelastic electron scattering at low values of q from electric low-lying vibrational levels in spherical nuclei ($60<A<150$ and $190<A<220$) has been fairly well described by a shape oscillation model devised by Tassie.[30,1] It provides explicit constructions for the transition charge density $\rho_L^{if}(r)$ and the transition convection current density $J_{cL,L\pm1}^{if}(r)$. At the high values of q which interest us, the nuclear spin magnetization should play an important role.[1] It is, however, not yet clear whether the transition spin currents are uniformly distributed over the nuclear volume, very localized, or characterized by some superposition of uniform and localized magnetization.[9,31]

As is well known,[1] the transition densities given by the Tassie model are:

$$\rho_L^{if}(r)=-D_L\hat{J}_f\,r(r/R)^{L-2}\,d\rho^G(r)/dr\,, \tag{20}$$

$$J_{cL,L-1}^{if}(r)=-i\omega D_L\hat{J}_f L^{-1/2}\hat{L}\,r(r/R)^{L-2}\rho^G(r), \tag{21}$$

and

$$J_{cL,L+1}^{if}(r)\equiv 0\,, \tag{22}$$

$$J_{cL,L}^{if}(r)\equiv 0\,, \tag{23}$$

where $\omega=E_i-E_f$ is the nuclear excitation energy, $\rho^G(r)$ the spherically symmetric nuclear ground-state charge density, and D_2 is a strength parameter to be determined empirically.

In the Tassie model (as well as in Bohr and Mottelson's rotational model) the velocity field

$$\vec{v}(\vec{r})=\sum_{lm}\beta_{lm}l^{1/2}\hat{l}\,r^{l-1}\,\vec{Y}_{l,l-1}^{m*}(\hat{r}),$$

which using Cartesian coordinates, can easily be seen to represent for $l=1$, $m=0$, a back and forth flow [shown in Fig. 1(a)], and for $l=2$, $m=0$, an elliptical volume-preserving motion [shown in Fig. 1(b)], is both irrotational and incompressible. $J_{cL,L}(r)$, the component of the convection current density which is responsible for magnetic transitions (representing an annular current), is zero.

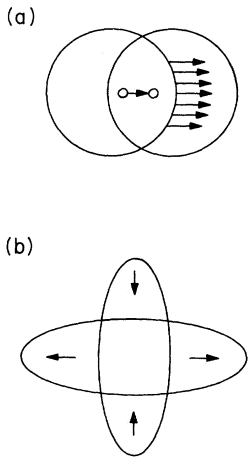

FIG. 1. Flow of nuclear charge in the Tassie model: (a) $l=1$, (b) $l=2$.

To permit magnetic transitions, we relax the constraint of irrotationality on $\vec{v}(\vec{r})$ so that $\vec{\nabla}\times\vec{v}(\vec{r})\neq 0$ and motion with vortices is possible. We assume, further, the existence of a transition convection current which reaches out over the entire nucleus instead of peaking near the nuclear surface. With $\rho_j(r)$ being a spherically symmetric current density close in shape to the ground-state charge density $\rho^G(r)$, the rotational component of the convection current is assumed to be given by a (volume-preserving) "roton" model

$$\vec{J}_c^{\,\mathrm{rot}}(\vec{r}) = iZ_{\mathrm{eff}}\,\rho_j(r)\sum_{lm}(\beta_{lm}/\mu_l)(r/R)^l\,\vec{Y}_{ll}^{m\,*}(\hat{r})\ ,$$

with β_{lm} the momentum and μ_l the mass of the roton, and where the strength of a nuclear transition can be adjusted to the experimental value by means of the parameter Z_{eff}. Pictorially, using Cartesian coordinates, the flow of this current is seen to correspond for $l=1$, $m=0$ to the uniform circulation shown in Fig. 2(a), and for $l=2$, $m=0$ to the twisting pattern of circulation of Fig. 2(b).

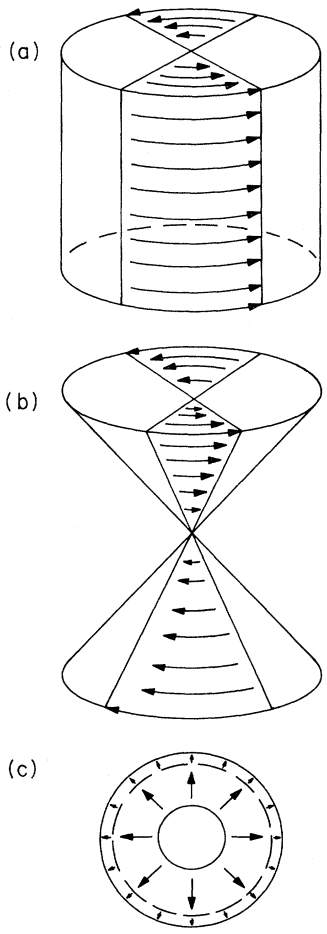

FIG. 2. Flow of nuclear charge in our incompressible rotational model: (a) $l=1$, (b) $l=2$; also in a compressible rotational model: (c) $l=0$ (breathing mode).

The above current leads to the density

$$J^{\mathrm{if}}_{cL,L}(r) = -Z_{\mathrm{eff}}\,(\tfrac{1}{2}\mu_L\omega_L)^{1/2}\rho_j(r)(\hat{J}_f/\mu_L)(r/R)^L\ , \tag{24}$$

ω_L being the roton frequency.

For completeness, the archetypal case of a compressible rotational fluid with a velocity field

$$\vec{v}(\vec{r}) = \sum_{lm}\beta_{lm}r^{l+1}\vec{Y}^{m\,*}_{l,l+1}(\hat{r})$$

is illustrated in Fig. 2(c) for $l=0$, $m=0$, where it is seen to constitute a breathing mode. For $l\geq 1$, the flow is difficult to illustrate.

To obtain a spin magnetization density supplementing the rotational current of Eq. (24), we postulate two simple models based on analogy with classical electrodynamics.[32]

MODEL I. The orbital motion of a charged particle gives rise to a magnetic moment $\vec{\mu}_c=(\frac{1}{2})\vec{r}\times\vec{J}_c$, and we assume that

$$\vec{\mu}_s(\vec{r}) = C\,\vec{\mu}_c(\vec{r})$$

for some constant C. From Eq. (24) we have

$$\vec{\mu}^{\,\mathrm{I}}_s(\vec{r}) = \tfrac{1}{2}iZ_{\mathrm{eff}}\rho_\mu(r) \times\sum_{lm}C_l(\beta_{lm}/\mu_l)(r/R)^l\,\vec{r}\times\vec{Y}^{m\,*}_{ll}(\hat{r})\ ,$$

where $\rho_\mu(r)$ is the magnetization density and C_l is a constant. If $\rho_\mu(r)$ comes from the unpaired nucleons in an outer shell, it will be peaked near the nuclear surface. Equation (16) can be used to calculate the spin current density:

$$J^{\mathrm{I}\,if}_{sL,L}(r) = \tfrac{1}{2}\hat{J}_f Z_{\mathrm{eff}}C_l(\omega_L/2\mu_L)^{1/2}(r/R)^L \times[(L+2)\rho_\mu(r)+r\,d\rho_\mu(r)/dr]\ . \tag{25}$$

MODEL II. Assume that the spin magnetization operator is given by the ansatz

$$\vec{\mu}^{\,\mathrm{II}}_s(r) = \sum_{lm}\rho_\mu(r)[A_{lm}f_l(r)\vec{Y}^{m\,*}_{ll+1}(\hat{r}) + B_{lm}\,g_l(r)\vec{Y}^{m\,*}_{ll-1}(\hat{r})]\ . \tag{26}$$

Assume further that $\vec{\mu}^{\,\mathrm{II}}_s=D\vec{\mu}_c$, with some constant D. We have $\vec{J}_c=\vec{\nabla}\times\vec{\mu}_c$, and thus:

$$\vec{\nabla}\times\vec{\mu}^{\,\mathrm{II}}_s(\vec{r}) = D\,\vec{\nabla}\times\vec{\mu}_c(\vec{r}) = D\,\vec{J}_c(\vec{r})\ .$$

The corresponding spin current density is

$$J^{\mathrm{II}\,if}_{sL,L}(r) = -\hat{J}_f Z_{\mathrm{eff}}D_L(\omega_L/2\mu_L)^{1/2}(r/R)^L\rho_\mu(r)\ . \tag{27}$$

The presence of $d\rho_\mu(r)/dr$ in Eq. (25) and its absence in Eq. (27) indicate that spin current in model I is much more concentrated near the nuclear surface.

In the same spirit, we can employ models I and II to obtain the transverse electric spin current density, this time starting with the irrotational convection current of the Tassie model.

MODEL I. Let

$$\vec{\mu}_s^{\,I}(\vec{r}) = \tfrac{1}{2}\rho_s(r) \sum_{lm} (-i\omega_l E_l \alpha_{lm} \hat{l}/l^{1/2}) \times r(r/R)^{l-2}\, \vec{r} \times \vec{Y}^{m*}_{l1-1}(\hat{r}), \tag{28}$$

$\rho_s(r)$ being another spin density function and E_l a constant, while α_{lm} is the collective roton "coordinate" variable. The corresponding spin current densities are

$$J^{I\,if}_{sL,L+1}(r) = (i\omega_L/2\hat{L})E_L D_L (L+1)^{1/2} \hat{J}_f \times r^2(r/R)^{L-2}\, d\rho_s(r)/dr \tag{29}$$

and

$$J^{I\,if}_{sL,L-1}(r) = [i\omega_L/2\hat{L}L^{1/2}]E_L D_L (L+1)\hat{J}_f\, r^2(r/R)^{L-2} \times [(\hat{L}^2/r)\rho_s(r) + d\rho_s(r)/dr]\,. \tag{30}$$

The same procedure can be applied to model II; the results will not be explicitly stated here.

V. RESULTS AND DISCUSSIONS

In this section we apply the eikonal method to an analysis of elastic and inelastic electron scattering from a variety of nuclei for high incident electron energies ($E_1 \geq 200$ MeV).

Based on the formalism developed in previous sections, we have written a computer code which permits the analysis of both elastic and inelastic scattering. The main computational difficulty encountered in developing this code was the choice of a numerical quadrature algorithm for integrating the oscillatory functions which appear in our final expressions for the scattering amplitudes, Eqs. (6)–(8). It was found that a modified Romberg method[33,34] worked reasonably well.

Elastic Coulomb scattering, especially from ^{208}Pb, ^{40}Ca, and its isotopes, has been thoroughly measured in recent years (for references up to 1971, see Überall[1]). Analysis of the data has revealed that at momentum transfers of $q \geq 3$ fm^{-1}, the smooth phenomenological charge distributions (modified Fermi or modified Gaussian) found satisfactory at lower values of q are no longer adequate.

Although we will work at large values of q, for the sake of simplicity we will use only the modified Fermi and modified Gaussian charge densities.

Comparatively little experimental data at high incident electron energies have been available for either inelastic scattering or elastic magnetic scattering from medium and heavy nuclei. According to Friar[35] the latest electron Linacs promise to allow measurements of cross sections at the 1% level or better for values of q^2 up to 15 fm^{-2}.

From parity and time-reversal arguments[1] we know that only the even Coulomb multipoles and odd magnetic multipoles contribute in the case of elastic scattering. In the extreme single-particle shell model (SPSM) the magnetic moment of a nucleus with a single valence nucleon is equal to that of the valence particle, due to pairing of nucleon spins. Donnelly and Walecka[5] have pointed out that orbitals with the highest j values in an oscillator shell should be well described by the SPSM.

A nucleus with ground-state spin J can have magnetic moments $M1$, $M3, \ldots ML$, where $L = 2J$. From an examination of the 6-J symbol in Eq. (19) we see that the orbital current density $J_{cLL}(r)$ vanishes if $L = 2j$ and $j = l + \frac{1}{2}$. Thus both for this case and also, of course, for the case of neutron orbitals only the spin current density $J_{sLL}(r)$ will contribute to the electron scattering cross section.

Since neutrons contribute little to charge scat-

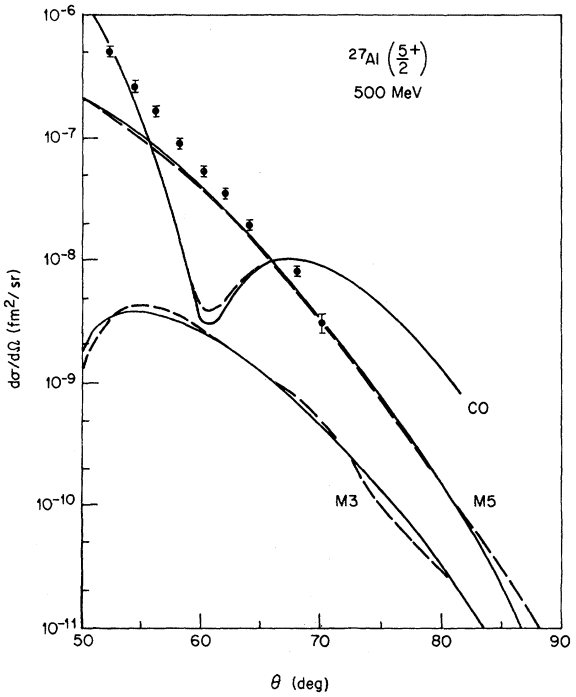

FIG. 3. Coulomb and higher magnetic moment elastic electron scattering cross sections from ^{27}Al based on a single-particle model. Solid lines: eikonal method; dashed lines: phase-shift analysis.

TABLE I. Elastic $M3$ cross section for ^{27}Al at 500 MeV incident electron energy.

θ (deg)	Eikonal results $d\sigma/d\Omega$ (fm^2/sr)	Phase-shift results a	b	c
50	2.14×10^{-9}	1.32×10^{-9}	1.28	1.28
52	3.61	2.96	3.12	3.13
54	4.25	4.37	4.58	4.58
56	4.14	4.75	4.76	4.76
58	3.58	4.07	3.94	3.94
60	2.85	3.00	2.91	2.91
62	2.15	2.11	2.12	2.12
64	1.55	1.52	1.58	1.58
66	1.09	1.14	1.17	1.17
68	7.42×10^{-10}	8.27×10^{-10}	8.20×10^{-10}	8.20×10^{-10}
70	4.96	5.42	5.22	5.22
72	3.24	3.13	3.05	3.05
74	2.07	1.68	1.71	1.71
76	1.27	9.27×10^{-11}	9.71×10^{-11}	9.71×10^{-11}
78	7.52×10^{-11}	5.56	5.73	5.74
80	4.21	3.56	3.47	3.48
82	2.20	2.20	2.06	2.07
84	1.05	1.19	1.15	1.15
86	4.51×10^{-12}	5.59×10^{-12}	5.80×10^{-12}	5.79
88	1.66	2.50	2.73	2.72
90	5.12×10^{-13}	1.23	1.29	1.29

[a] Phase-shift results (Ref. 7); 35 partial waves; integration step size 0.02 fm inside the 0.03 fm outside the interaction radius (taken as 11.26 fm).

[b] Phase-shift results; 40 partial waves; step size 0.02/0.03 fm.

[c] Phase-shift results; 40 partial waves; step size 0.03/0.05 fm.

TABLE II. Elastic $M5$ cross section for ^{27}Al at 500 MeV incident electron energy.

θ (deg)	Eikonal results $d\sigma/d\Omega$ (fm^2/sr)	Phase-shift results [a]
50	3.46×10^{-7}	3.16×10^{-7}
52	2.37	2.22
54	1.59	1.52
56	1.04	1.01
58	6.65×10^{-8}	6.55×10^{-8}
60	4.19	4.15
62	2.59	2.57
64	1.59	1.56
66	9.58×10^{-9}	9.34×10^{-9}
68	5.72	5.48
70	3.37	3.15
72	1.96	1.78
74	1.11	9.83×10^{-10}
76	6.17×10^{-10}	5.37
78	3.31	2.90
80	1.70	1.55
82	8.27×10^{-11}	8.22×10^{-11}
84	3.77	4.29
86	1.60	2.21
88	6.27×10^{-12}	1.12
90	2.31	5.66×10^{-12}

[a] Phase-shift results (Ref. 7); 35 partial waves, integration step size 0.02 fm inside and 0.03 fm outside the interaction radius (taken as 11.26 fm).

tering, it is elastic magnetic scattering that may be used for investigating neutron distributions in the nuclear ground state.

We now consider a number of different nuclei having higher magnetic multipole moments.

$$^{27}_{13}\mathrm{Al}(\tfrac{5}{2}^{+})$$

The single-particle configuration is taken as $(1d_{5/2})^{-1}{}_p$, a proton hole in $^{28}_{14}$Si, and $M1$, $M3$, and $M5$ multipoles are possible. Since $j=l+\frac{1}{2}$ (the so-called "stretch case"), only the spin magnetization will contribute to the $M5$ cross section. The harmonic oscillator parameter b and the Fermi charge density parameters c and t have been taken from a recent phase-shift analysis.[7] They are $b=1.8$ fm, $c=2.82$ fm, and $t=2.43$ fm.

In Fig. 3, we present our results for the $C0$, $M3$, and $M5$ scattering cross sections (in units of fm^2/sr). For purposes of comparison (using the computer code described in Ref. 7) we have also computed the corresponding phase-shift cross sections using the same nuclear model. In the figure, the phase-shift calculations performed at an incident electron energy of 500 MeV use 35 partial waves. Numerical values of the $M3$ and $M5$ cross sections are given in Tables I and II, showing also the dependence on the number of phase shifts and the integration step size chosen. (Note that the undulations in the $M3$ phase-shift curve persist as the number of phase shifts is increased from 35 to 40, indicating that they may not be caused by a lack of convergence of the phase-shift series.)

The measured points in Fig. 3 are taken from Ref. 3. There appears to be close agreement between the eikonal (solid lines) and phase-shift $C0$ and $M5$ cross sections (dashed lines). A frequent feature of the eikonal results (noted previously in charge scattering cross sections[22]) is the fact that the eikonal diffraction minima are deeper (closer to the PWBA zeros) than those from the phase-shift results.

Both methods of calculation show that the magnetic scattering cross section may actually exceed the charge monopole cross section at angles much less than 180° (e.g. near $\theta=60°$). From these and other results it will become clear that given the

right choice of incident energy, angular regions can be found where the magnetic cross section is measurable.

Very close to $\theta = 180°$, the charge cross section always falls steeply to zero. If elastic cross sections of the order of 10^{-12} fm^2/sr are measurable today[36] then the magnetic cross section should, in any case, be frequently measurable near 180°.

It should be noted that in every instance both center-of-mass and finite-nucleon-size corrections have been ignored. Since the partial-wave computer code used[7] does not contain such corrections we will omit them in our calculations whenever we are making a direct comparison with phase-shift results. Thus, unless it is explicitly stated to the contrary, all SPSM calculations in this paper will use uncorrected harmonic oscillator (HO) wave functions. However, at very high values of q these corrections are significant, as we will later demonstrate.

$^{51}_{23}\mathrm{V}(\frac{7}{2}^-)$

The single-particle model assigns a configuration of $(1f_{7/2})^3_p$ to the valence particle in Vanadium. Assuming the normal coupling of spins, we then have a stretched configuration $(1f_{7/2})_p$ with the possibility of $M1$, $M3$, $M5$, and $M7$ multipole contributions. We will use a harmonic oscillator parameter[7] $b = 2.01$ fm, and for the ground-state charge density a Fermi density with $c = 3.95$ fm and $t = 2.24$ fm.

The charge and $M7$ cross sections, as calculated by the eikonal (solid curves) and phase-shift methods, along with measurements taken by Peterson *et al.*[37] are presented in Fig. 4 for $E_1 = 250$ MeV.

From these figures we see (1) the close correspondence between the eikonal and phase-shift results, and (2) the large size of the $M7$ cross section relative to its charge counterpart in the neighborhood of $\theta = 90°$.

The fact that the eikonal and phase-shift $M7$ cross sections in Fig. 4 are starting to separate around $\theta = 90°$ will be discussed later.

$^{209}_{83}\mathrm{Bi}(\frac{9}{2}^-)$

This nucleus has a $1h_{9/2}$ proton outside the ^{208}Pb core. Since $j = l - \frac{1}{2}$ in this case, both the orbital and spin magnetizations will contribute to the $M9$ cross section. A measurement of $F_T^2(q)$ for $M9$ at one single point[3] has indicated the feasibility of more thorough experimental investigation of bismuth's higher magnetic moments. Bertozzi[36] has shown in PWBA that using configuration mixing to improve the bismuth ground-state wave function, rather than using SPSM as in Ref. 3, lessens the disagreement between theory and the single experimental point.

We have computed the charge monopole cross

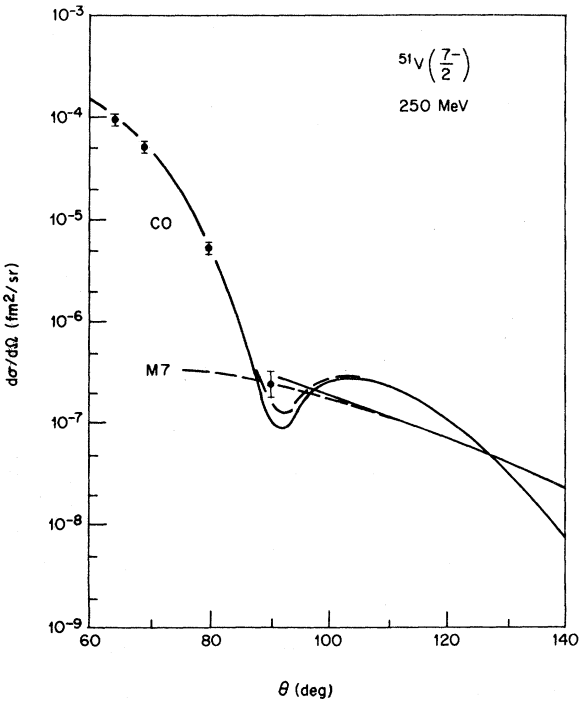

FIG. 4. Same as Fig. 3, for a ^{51}V target.

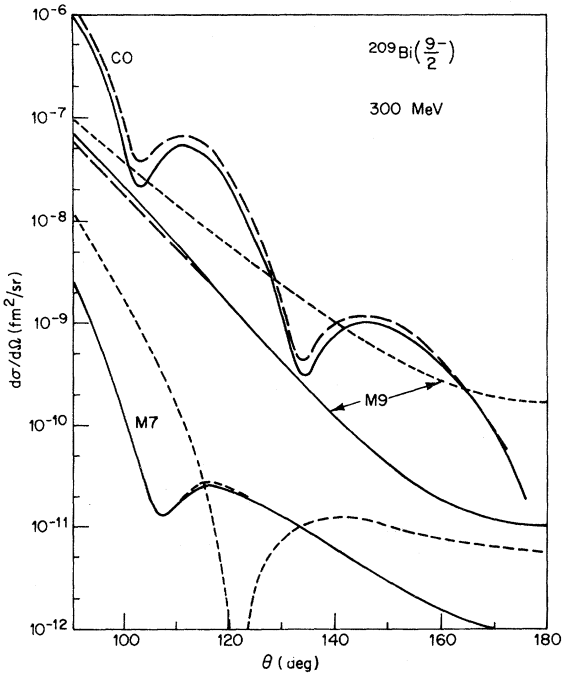

FIG. 5. Same as Fig. 3, for a ^{209}Bi target. Dotted lines: plane-wave Born approximation.

TABLE III. Elastic $M7$ cross section for ^{209}Bi at 300 MeV incident electron energy.

θ (deg)	Eikonal results $d\sigma/d\Omega$ (fm^2/sr)	Phase-shift results [a]
90	2.73×10^{-9}	2.57×10^{-9}
92	1.61	1.53
94	9.14×10^{-10}	8.66×10^{-10}
96	4.91	4.66
98	2.48	2.35
100	1.16	1.10
102	5.06×10^{-11}	4.88×10^{-11}
104	2.25	2.26
106	1.37	1.46
108	1.37	1.49
110	1.67	1.80
112	2.00	2.10
114	2.22	2.31
116	2.32	2.38
118	2.31	2.35
120	2.20	2.22
122	2.04	2.05
124	1.85	1.84
126	1.64	1.63
128	1.44	1.43
130	1.25	1.24
132	1.08	1.06
134	9.23×10^{-12}	9.11×10^{-12}
136	7.89	7.78
138	6.74	6.65
140	5.75	5.68
142	4.92	4.86
144	4.22	4.18
146	3.63	3.60
148	3.14	3.12
150	2.73	2.72
152	2.38	2.38
154	2.10	2.10
156	1.86	1.86
158	1.66	1.67
160	1.50	1.51
162	1.36	1.37
164	1.25	1.26
166	1.16	1.17
168	1.08	1.10
170	1.02	1.04
172	9.74×10^{-13}	9.89×10^{-13}
174	9.39	9.55
176	9.14	9.31
178	9.00	9.17
180	8.95	

[a] Phase-shift results (Ref. 7); 30 partial waves; integration step size 0.05 fm throughout.

TABLE IV. Elastic $M9$ cross section for ^{209}Bi at 300 MeV incident electron energy.

θ (deg)	Eikonal results $d\sigma/d\Omega$ (fm^2/sr)	Phase-shift results [a]
90	6.24×10^{-8}	5.47×10^{-8}
92	5.08	4.53
94	4.10	3.71
96	3.28	3.01
98	2.60	2.41
100	2.05	1.92
102	1.61	1.52
104	1.25	1.19
106	9.72×10^{-9}	9.26×10^{-9}
108	7.50	7.18
110	5.78	5.55
112	4.44	4.27
114	3.40	3.28
116	2.60	2.52
118	1.99	1.93
120	1.53	1.48
122	1.17	1.14
124	9.01×10^{-10}	8.76×10^{-10}
126	6.95	6.76
128	5.38	5.24
130	4.18	4.07
132	3.26	3.18
134	2.56	2.50
136	2.02	1.98
138	1.61	1.57
140	1.29	1.26
142	1.04	1.02
144	8.44×10^{-11}	8.30×10^{-11}
146	6.93	6.82
148	5.73	5.65
150	4.79	4.73
152	4.05	3.99
154	3.45	3.41
156	2.97	2.94
158	2.59	2.56
160	2.28	2.25
162	2.03	2.00
164	1.83	1.81
166	1.67	1.64
168	1.54	1.52
170	1.44	1.41
172	1.36	1.34
174	1.30	1.28
176	1.26	1.24
178	1.24	1.21
180	1.23	

[a] Phase-shift results (Ref. 7); 30 partial waves; integration step size 0.05 fm throughout.

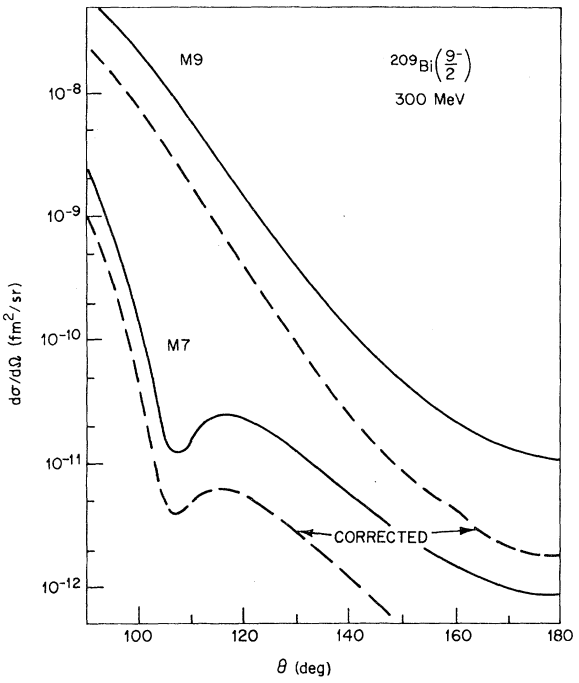

FIG. 6. Eikonal cross sections for ^{209}Bi, uncorrected (solid lines) and with Tassie-Barker recoil and proton-size correction (dashed lines).

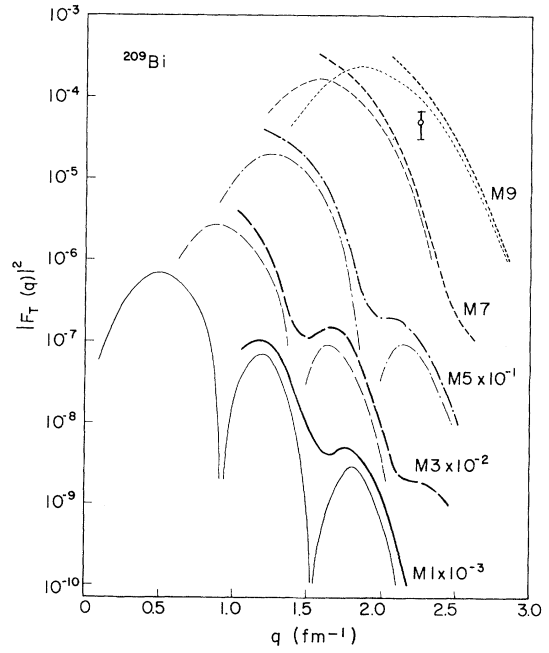

FIG. 7. Squared eikonal multipole "form factors" (elastic cross section divided by Mott cross section) drawn as heavy curves, and Born form factors drawn as light curves for ^{209}Bi, calculated at 500 MeV. Experimental point taken from Ref. 3. Nucleon size and center-of-mass corrections are included. Eikonal curves stop at the limit of their validity at left (see end of Sec. V).

section and magnetic multipole cross sections at various energy values of the incident electron. The bismuth ground-state charge density is modeled with a Fermi density where $c = 6.7087$ fm and $t = 2.1271$ fm. The harmonic oscillator parameter b is 2.33 fm.

At an incident electron energy of 300 MeV we have calculated the eikonal (solid curves) and phase-shift $C0$, $M7$, and $M9$ shown in Fig. 5. The $M7$ and $M9$ phase-shift cross sections are in particularly good agreement with the corresponding eikonal results; this is also indicated numerically in Tables III and IV. The PWBA $M7$ and $M9$ cross sections (short dashed lines) serve to emphasize the large effect of Coulomb distortion.

We have recomputed the eikonal $M7$ and $M9$ cross sections in Fig. 6; this time we have taken into account the finite nucleon size and nucleon recoil by using the standard Tassie-Barker correction factor.[1] The effect of this correction is clearly visible.

The eikonal approximation should increase in validity as the incident electron's energy is raised. Since partial-wave analyses become less accurate and more lengthy as the number of contributing partial waves increases, our method becomes particularly useful for say $E_1 > 300$ MeV. However, we see from Fig. 7 that the eikonal transverse

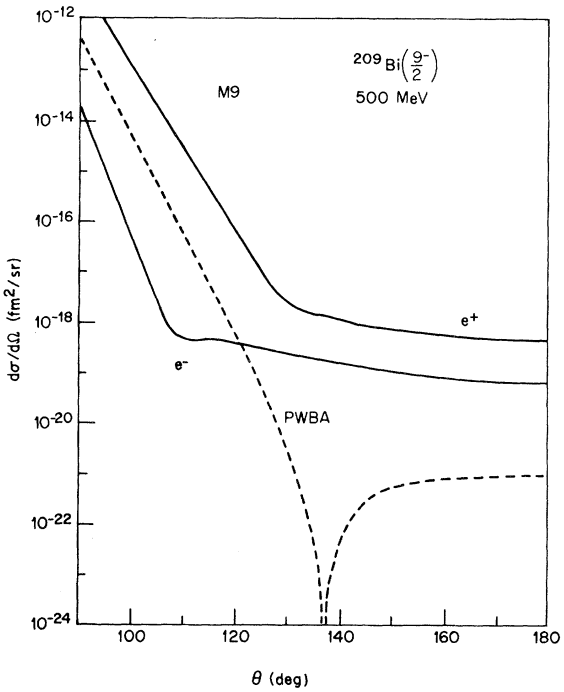

FIG. 8. Elastic $M9$ electron and positron cross sections of ^{209}Bi, calculated by eikonal (solid lines) and Born (common dashed line) approximation.

form factor (calculated at $E_1 = 500$ MeV and defined in the same manner as its PWBA counterpart[1]) starts to sharply deteriorate at low q values. As the multipolarity L is raised the region of validity (in q) decreases. Evidently, the phase-shift calculations are needed to cover the complete range of q values.

It is interesting to note from Fig. 8 that the $M9$ positron cross section is one or several orders of magnitude larger than the $M9$ electron cross section.

In situations where one wishes to vary the incident energy of the electron, one must rerun a partial-wave code for each incident energy value. This is a time-consuming process. Most of the computation time in a phase-shift analysis of electron scattering is taken up in performing the radial integrations.[9,38] Should the incident energy be changed, the integrations have to be repeated *ab initio*. The $M9$ cross sections in Fig. 9, calculated at fixed q and θ by the eikonal method where such is not the case, illustrate a particular advantage of this approach.

Let us define the magnetic form factor by

$$|F(q)|^2 = (d\sigma/d\Omega)/\sigma_M \qquad (31)$$

with σ_M the Mott cross section. Employing the eikonal formalism and corrected HO nuclear wave functions, we illustrate the (E_1, q) dependence of representative DWBA magnetic form factors in Fig. 10.

The $M1$ form factor is given for various values of E_1 as q ranges from 1.5 fm^{-1} to 2.5 fm^{-1}. The dependence of this form factor on the incident energy of the electron (which is absent in PWBA) is striking. Redefining the magnetic form factor so that the denominator in Eq. (31) includes the kinematic quantity $(\frac{1}{2}+\tan^2\theta/2)$, the $M9$ form factor in Fig. 9 is evidently still dependent on the incident electron energy.

$^{208}_{82}$Pb

Coulomb elastic electron scattering experiments[39] on ^{208}Pb have shown that a modified Gaussian charge density with an oscillating function tacked onto it can closely fit measured data up to $\theta = 70°$ at 502 MeV.

The 2.61 MeV 3^- level has been extensively studied.[13,40,41] Data up to $q = 3$ fm^{-1} indicate (1) that at least for $r \geq 2$ fm, $\rho_L^{if}(r)$ has oscillating components, and (2) this level is highly collective.

In Fig. 11 we present the eikonal (solid line) and phase-shift cross sections (unnormalized) for electron scattering from this level at $E_1 = 502$ MeV. The ground-state charge density $\rho^G(r)$ is a modified Gaussian with parameters taken from Ref. 13, i.e., $c = 6.3032$ fm, $z = 2.888$ fm, and $w = 0.338$. The transition charge density is given by the Tassie model

$$\rho_L^{if}(r) = r^{L-1}(d/dr)\rho^G(r; c_{tr}, z_{tr}),$$

where w is now set equal to zero, $c_{tr} = 6.25$ fm, and $z_{tr} = 2.93$ fm. The partial-wave calculations were performed with the electric partial-wave code HEINEL.[13] The position (in q) and shape of

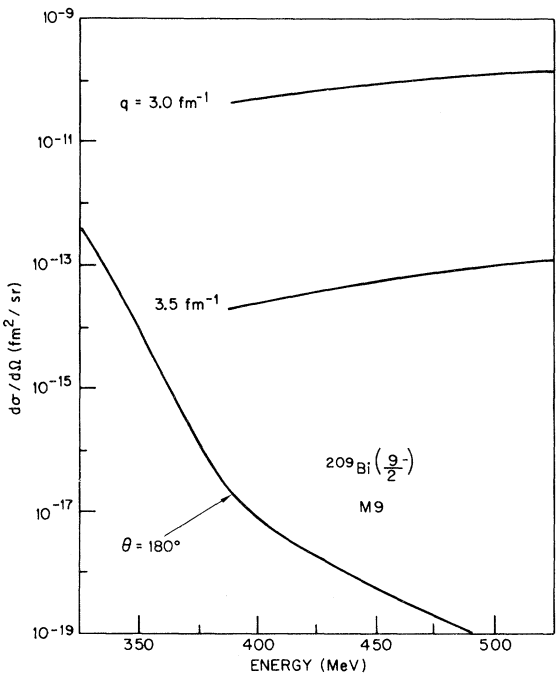

FIG. 9. Energy dependence of elastic $M9$ cross section of ^{209}Bi at fixed values of q or of θ.

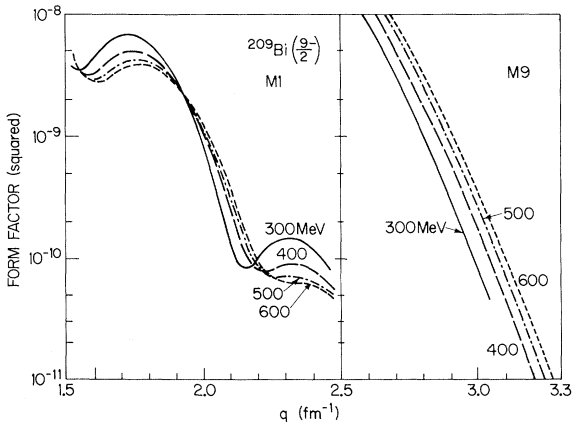

FIG. 10. Eikonal $M1$ and $M9$ "form factors" of ^{209}Bi and their energy dependence. The latter is a measure of the Coulomb distortion since the corresponding Born form factors are energy-independent.

the eikonal diffraction curves are seen to match the phase-shift results very well.

The reason for the rapid oscillations in the partial-wave cross section for $q > 4.5$ fm^{-1} is unclear. Forty partial waves were used in the calculation.

$^{115}_{49}$In

Chertok and Johnson[42] have calculated mixing ratios and deduced spins and parities associated with levels in ^{115}In for extremely low (threshold) incident electron energies. They employed a version of the Duke[43] partial-wave code which assumed that the magnetic transition density was purely orbital and given by

$$J^{if}_{cL,L}(r) \sim r^{L-1}\, d\rho^G(r)/dr \ ,$$

where $\rho^G(r)$ is the (Fermi) ground-state charge density. Since they were concerned with a model-independent calculation—feasible at such low electron energies—this simple model was adequate.

In Fig. 12 we show the PWBA (dotted lines) and eikonal cross sections at $E_1 = 500$ MeV for scattering from the 1.46 MeV level in ^{115}In. The parameters of the Fermi ground-state charge density, $c = 5.24$ fm and $t = 2.3$ fm are taken from Ref. 1. For illustrative purposes we have assumed that this is a pure spin-flip $M1$ transition, i.e., the orbital current does not contribute at all. A Fermi density with $c = 5.4$ fm and $t = 2.2$ fm is used to model the spin magnetization density in both Eqs. (25) and (27). We see that the diffraction minima for model II are displaced relative to those for model I.

From the examples we have discussed we see that for smaller scattering angles the eikonal cross section becomes progressively more inaccurate (it grows rapidly as θ decreases). Near a diffraction maximum one can always locate the limit point below which the eikonal formalism breaks down by computing the PWBA cross section. For a given $q'R$, the inaccuracy increases as the multipolarity L is raised.

The reason for this inaccuracy lies in the fact that for forward angles, some terms in the eikonal expansion such as $R(r, \epsilon)$ defined after Eq. (6), which enters the amplitude through $E^{-\nu-1}$, are no longer small compared to unity. This difficulty arises from the basic eikonal method which expands deviations from plane waves in powers of r, cf. Eqs. (2) and (3).

It seems probable that by not using the asymptotic integration over μ this type of error could have been rendered less significant. However, as remarked by Yennie *et al.*[21] (and it still remains true today), a numerical evaluation of the scat-

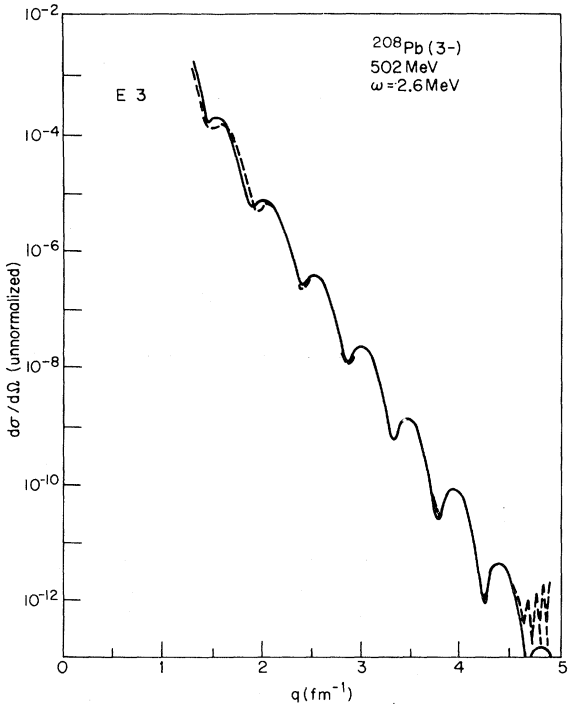

FIG. 11. Inelastic cross section for the 3$^-$ level of ^{208}Pb at 502 MeV, obtained by eikonal (solid line) and phase-shift (dashed line) methods.

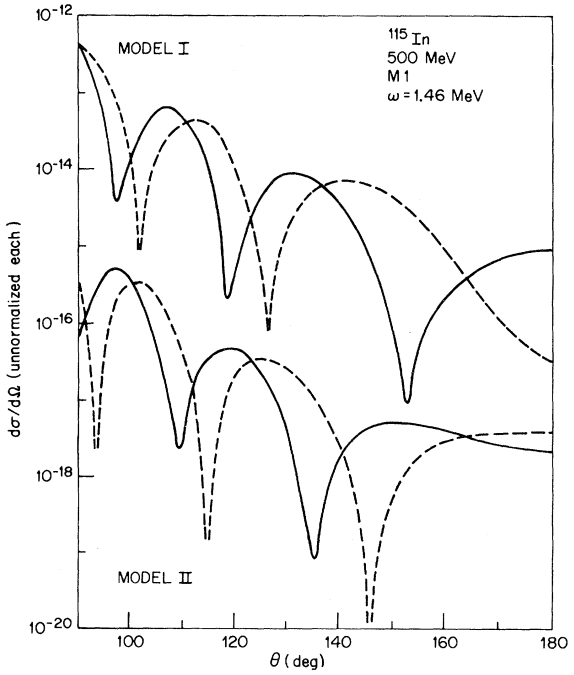

FIG. 12. $M1$ transitions in ^{115}In, obtained by eikonal (solid lines) and Born (dashed lines) methods on the basis of two collective models for magnetic transitions as discussed in the text.

tering amplitude avoiding completely the asymptotic integration over the angular variable μ, seems profitless due to the very large amount of computer time that a three-dimensional integral would consume.

Another source of error is the fact that we have retained only the first-order spinor $u^0(\vec{r}_e)$ and the first-order term in a Taylor series expansion of the eikonal function $S(\vec{r}_e)$. McDonald[44] has shown that for charge scattering from a uniform density, inclusion of the second-order terms in $S(\vec{r}_e)$ and in the spinor $u(\vec{r}_e)$ produces only a slight improvement in the accuracy of the cross section.

VI. SUMMARY AND CONCLUSIONS

Comparisons of eikonal and phase-shift electron-nucleus scattering cross sections for incident-electron energies above 200 MeV have shown that this high-energy approximation can accurately calculate Coulomb distortion under certain conditions.

When measured data for transverse scattering cross sections from medium or heavy nuclei at high values of q (say $q > 2$ fm^{-1}) become available, this method should be reasonably accurate for testing models of the nuclear charge and current densities.

We have seen that for low values of $q'R$ the method becomes inapplicable. For small scattering angles, even at high incident electron energies, only a partial-wave analysis can compute the effect of Coulomb distortion. However, at the present time, the eikonal approach appears to be particularly useful for high-energy magnetic electron scattering (both elastic and inelastic) and large scattering angles. The limits of applicability in (E_1, θ, L) of a recently developed phase-shift code ZENITH[45] are unknown to the present authors.

ACKNOWLEDGMENTS

We wish to thank Dr. L. J. McDonald for valuable discussions. Dr. T. Provost and Dr. J. Heisenberg of MIT provided us with a copy of the phase-shift code HEINEL and gave us assistance in its execution. Dr. L. E. Wright of Ohio University did the same with his partial-wave code MAGEL. The help of Dr. Nino Bonavito of Goddard Space Flight Center in regard to the numerical calculations has been invaluable.

---

*Work supported in part by a grant of the National Science Foundation.

[1]H. Überall, *Electron Scattering from Complex Nuclei, Parts A and B* (Academic, New York and London, 1971).
[2]T. W. Donnelly, Phys. Rev. C 1, 833 (1970).
[3]G. C. Li, I. Sick, J. D. Walecka, and G. E. Walker, Phys. Lett. 32B, 317 (1970).
[4]J. D. Murphy and H. Überall, Phys. Lett. 44B, 347 (1973).
[5]T. W. Donnelly and J. D. Walecka, Nucl. Phys. A201, 81 (1973).
[6]L. E. Wright and J. F. Prewitt, in *Proceedings of the International Conference on Photonuclear Reactions and Applications, Asilomar, March 1973,* edited by B. L. Berman (Lawrence Livermore Laboratory, Univ. of California, 1973), p. 2C8-1.
[7]J. F. Prewitt and L. E. Wright, Phys. Rev. C 9, 2033 (1974).
[8]L. Lapikas, A. E. L. Dieperink, and G. Box, Nucl. Phys. A203, 609 (1973).
[9]D. Drechsel, Nucl. Phys. A113, 665 (1968).
[10]W. W. Gargaro and D. S. Onley, J. Math. Phys. 11, 1191 (1970).
[11]W. W. Gargaro and D. S. Onley, Phys. Rev. C 4, 1032 (1971).
[12]N. Glossmann and C. Toepffer, Nucl. Phys. A161, 330 (1971).
[13]J. Heisenberg and I. Sick, Phys. Lett. 32B, 249 (1970).
[14]See for example, M. Born and E. Wolf, *Principles of Optics* (Pergamon, New York, 1959).
[15]L. I. Schiff, Phys. Rev. 103, 443 (1956).
[16]D. S. Saxon, Phys. Rev. 107, 871 (1957).
[17]D. S. Saxon and L. I. Schiff, Nuovo Cimento 6, 614 (1957).
[18]J. J. Tiemann, Ph.D. thesis, Stanford University, 1960 (unpublished).
[19]R. J. Glauber, in *Lectures in Theoretical Physics* (Interscience, New York, 1959), Vol. I, p. 315.
[20]A. Baker, Phys. Rev. 134, B240 (1964).
[21]D. R. Yennie, F. L. Boos, Jr., and D. G. Ravenhall, Phys. Rev. 137, B882 (1965).
[22]I. Zh. Petkov, V. K. Luk'yanov, and Yu. S. Pol', Yad. Fiz. 4, 57 (1966) [transl.: Sov. J. Nucl. Phys. 4, 41 (1967)].
[23]I. Zh. Petkov, V. K. Luk'yanov, and Yu. S. Pol', Yad. Fiz. 4, 556 (1966) [transl.: Sov. J. Nucl. Phys. 4, 395 (1967)].
[24]V. K. Luk'yanov, I. Zh. Petkov, and Yu. S. Pol', Yad. Fiz. 9, 349 (1969) [transl.: Sov. J. Nucl. Phys. 9, 204 (1969)].
[25]Yu. S. Pol', Yad. Fiz. 10, 771 (1969) [transl.: Sov. J. Nucl. Phys. 10, 445 (1970)].
[26]V. K. Luk'yanov and Yu. S. Pol', Yad. Fiz. 11, 556 (1970) [transl.: Sov. J. Nucl. Phys. 11, 312 (1970)].
[27]J. T. Reynolds, Ph.D. thesis, Duke University, 1964 (unpublished).
[28]F. Scheck, Nucl. Phys. 77, 577 (1966).
[29]T. DeForest and J. D. Walecka, Advan. Phys. 15, 1 (1966).
[30]L. J. Tassie, Aust. J. Phys. 9, 407 (1956).
[31]B. T. Chertok, Phys. Rev. 187, 1340 (1969).

[32]J. D. Jackson, *Classical Electrodynamics* (Wiley, New York, 1962).
[33]W. R. Bunton, M. Diethelm, and K. Haigler, Jet Propulsion Laboratory, Pasadena, California, Technical Memorandum No. 314-221, 1969 (unpublished).
[34]E. K. Miller, J. Comput. Phys. 5 (1970).
[35]J. L. Friar, Ann. Phys. (N.Y.) 81, 332 (1973).
[36]W. Bertozzi, in Proceedings of the NATO Advanced Institute on Electron Scattering and Nuclear Structure, Santa Margherita di Pula, Cagliari, Sardinia, September 1970, edited by B. Bosco (Gordon and Breach, New York) (to be published).
[37]G. A. Peterson, K. Hosoyama, M. Nagao, A. Nakada, and Y. Torizuka, Phys. Rev. C 7, 1028 (1973).
[38]J. F. Ziegler, Yale University, New Haven, Connecticut Report No. YALE-2726E-49 (unpublished).
[39]J. Heisenberg, R. Hofstadter, J. S. McCarthy, I. Sick, B. C. Clark, R. Herman, and D. G. Ravenhall, Phys. Rev. Lett. 23, 1402 (1969).
[40]J. P. Ziegler and G. A. Peterson, Phys. Rev. 165, 1337 (1968).
[41]J. Friedrich, Nucl. Phys. A191, 118 (1972).
[42]B. T. Chertok and W. T. K. Johnson, Phys. Rev. 174, 1525 (1968).
[43]S. T. Tuan, L. E. Wright, and D. S. Onley, Nucl. Instrum. Methods 60, 70 (1968).
[44]L. McDonald, M. S. thesis, University of Minnesota, 1965 (unpublished).
[45]R. L. Mercer and D. G. Ravenhall, Phys. Rev. C 10, 2002 (1974).